9B.1 RANGE-VELOCITY MITIGATION VIA SZ PHASE CODING WITH EXPERIMENTAL S-BAND RADAR DATA

J.C. Hubbert*, G. Meymaris and R.J. Keeler
National Center for Atmospheric Research, Boulder CO

1. Introduction

A fundamental limitation of pulsed weather radar is range-velocity ambiguity which is expressed by the equation $r_a v_a = c\lambda/8$ where r_a, v_a are the unambiguous range and velocity, respectively, for wavelength λ and where c is the speed of light. Since the product $r_a v_a$ is constant for a particular wavelength, increasing either one (r_a or v_a) necessarily decreases the other. For $\lambda = 10\,\text{cm}$ (S-band) and a typical pulse repetition time (PRT) of 1 ms, $r_a = 150\,\text{km}$ and $v_a = 25\,\text{m/s}$. Weather phenomena routinely exceed both of these limits. SZ phase coding of the transmit pulses for single polarization radars has been shown to be an effective method for the separation of range overlaid echoes thus extending r_a without compromising v_a (Sachidananda and Zrnić 1999, referred to as SZ99 from here on). To date statistical performance of phase coding has been shown only for simulated Gaussian shaped weather spectra. It is well known that weather spectra shapes can deviate significantly from Gaussian and thus statistical analysis should done for experimental spectra. The difficulty in performing a quantitative analysis on experimentally obtained data for the SZ phase coding technique is the lack of precise truth for comparison. It is not possible for a radar to simultaneously collect data of both overlaid and non-overlaid signals for the same range gate. The current solution has been to scan the same region twice: once to collect coded, overlaid data (transmitting SZ(8/64), short PRT) and once for non-overlaid uncoded data (transmitting no phase shifts, long PRT). The temporal discrepancy in measurement time intervals is a source of error that will degrade the evaluation of the algorithm. Frush et al. (2000) have analyzed experimentally gathered phase coded data. The time separation between the collected phase coded and uncoded data scans was six minutes which made comparisons difficult and qualitative. Thus, to date no definitive quantitative evaluation of the SZ phase coding technique has been done for experimentally gathered data. In this paper the SZ phase coding algorithm is evaluated with experimental weather time series that are not phase coded. The time series are phase coded offline as either a first or second trip echo and then combined, thus simulating experimentally gathered phase coded data.

*ATD/NCAR, Boulder, Colorado 80307, email: hubbert@ucar.edu

2. Background

The theory of SZ(8/64) phase coding is covered in SZ99. When the first trip (considered the strong trip here) echoes are made coherent, the second trip is phase shifted by the SZ(8/64) *modulation code* (times series considered here are 64 in length). The spectrum of the phase modulated second trip consists of eight replicas of the spectrum of the unphase coded second trip echo. To recover the moments of the weak trip signal, at least two of these replicas need to be preserved. Thus 3/4 of the weak trip spectrum can be "notched" or zeroed and this 3/4 notch is typically centered at the mean velocity of the coherent first trip. An attractive feature of the SZ phase code is that the auto covariance function of the phase code sequence is 1 for lags 0, 7, 15 etc., and zero otherwise. Thus velocity estimates of the first trip coherent signal are unbiased by the overlaid modulated second trip echo.

The signal processing steps in executing the SZ(8/64) algorithm on unphase coded data are as follows: (moments with "^" are recovered while others without "^" are "truth" calculated from the original time series): 1) Phase code two time series, one as first trip the other as second trip and combine the sequences, 2) Create two sequences by cohering the combined sequence for the first and then second trip echoes, 3) Calculate $|R(1)|$ (first lag autocovariance) for both sequences; the greater one determines which trip is stronger, 4) Calculate the power $\hat{P}_1$, velocity $\hat{V}_1$ and width $\hat{W}_1$ for the stronger trip (always referred to with the subscript "1" but not necessarily the first trip), 4) Apply Hanning window to the combined time series and correct for the power loss, 5) Transform into the frequency domain via an FFT algorithm, 6) Apply 3/4 notch filter centered at the $\hat{V}_1$ estimated velocity, 7) Calculate the weaker trip power, $\hat{P}_2$, from the notched spectrum and multiply by 4 to account for the effects of the 3/4 notch, 8) If the recovered power ratio $P_1/P_2 < 20\,\text{dB}$, $\hat{P}_1$ is corrected by subtracting $\hat{P}_2$, 9) Transform the notched spectrum back to the time domain (via an IFFT)

and cohere to the weaker trip, 10) Calculate $\hat{V}_2$, and 11) Estimate the weaker trip spectrum width via the deconvolution method given in SZ99.

1. Data Analysis

The data was collected on several NEXRAD radars. A total of 5,300 I&Q time series (64 samples each) were selected from 2 short-PRT PPI scans, categorized by hand, and then stored in a database. The existence of clutter, weather, and multi-modal weather signals were established by a human expert and stored with the time series. All the time series were then paired with every other time series to create another database with over 14 million data blocks (5,300 choose 2 possible combinations). Each of these data blocks was created by phase coding the stronger of the pair for trip 1, the other for trip 2, and then combining the pair, thus simulating overlaid echoes. As done in SZ99, we show only the standard deviation of the velocity of the weaker trip and then compare our results to SZ99. Shown in Fig. 1 is the standard deviation of the error (SDE) for the recovered moment $\hat{V}_2$ as a function of P_1/P_2 and W_1 with $3.75\,\mathrm{m/s} < W_2 < 4.25\,\mathrm{m/s}$ (Nyquist vel.= 32m/s). If a SDE of 2.5 m/s is acceptable, the recovery region for $\hat{V}_2$ is about $P_1/P_2 < 35\,dB$ at $W_1 = 0\,\mathrm{m/s}$ and decreases with increasing W_1. This is expected since as W_1 increases the amount of strong trip signal remaining in the weak trip spectrum after notch filtering will also increases thus effectively reducing the SNR of the weak trip echo . In general, the SDE of $\hat{V}_2$ does decrease for narrower spectral widths but the upper limit for recovery is always about $P_1/P_2 = 35\,dB$. The statistics above 4 m/s are not valid due to under sampling of spectra with $W > 4\,\mathrm{m/s}$.

Next these results are compared to the results obtained via numerical simulation in SZ99. Shown in Fig. 2 is the SDE of $\hat{V}_2$ from SZ99 for the same parameters as used in Fig. 1. As can be seen, the SDE from our experimental data in Fig. 1 are in general larger those from simulated data in SZ99. The largest discrepancy occurs for values of W_1 of 3 m/s and larger. This comparison suggest that the SZ(8/64) algorithm may not perform as well, in terms of variance of recovered $\hat{V}_2$, as indicated in SZ99. This is likely due to the experimental spectra not being Gaussian shaped and is illustrated by the not untypical weather spectrum shown in Fig. 3 with the fitted Gaussian curve overlaid. The energy outside the Gaussian curve will increase the leakage of the strong trip echo into the weak trip recovery spectra, thus degrading the performance the SZ(8/64) algorithm.

Next, two unphase coded PPI scans are phase coded as first and second trip echoes, overlaid and then the moments are recovered. The spatial concatenation of the unphase coded PPI scans gives truth for the recovered moments. Figures 4 and 5 (bottom panels) show SZ(8/64) recovered raw power (I^2+Q^2) and radial velocity, respectively, and can be compared directly to the truth field in the top panel of each figure. The recovery is quite good wherever there is significant power in both trips. However, if there is little or no power in the weaker trip, and the stronger trip has a wide spectrum width the stronger trip can leak through to the weaker trip. This can be seen in the lower left quadrants of Figs. 4 and 4 (bottom panels). Here, the "speckle" in the mean velocity field should be an excellent indicator of of leakage from the stronger trip so that the data could be censored automatically using a spatial velocity variance estimator. For comparison, the velocity field as would be measured by the current WSR-88D short PRT collection scheme is constructed from the truth data of Figs. 4 and 5 and is shown in Fig. 6. The region in white is the area where the velocities are censored due to overlaid echoes. The increase in the amount of good velocity estimates available in SZ recovered velocity field shown in Fig. 5 is dramatic.

Censoring of poor quality data is essential for an operational application of the SZ phase coding scheme. The obvious variables for censoring are P_1, P_2 and W_1. Current NEXRAD implementation plans call for two scans at the lowest two elevation angles: 1) a long PRT (≈ 3.1 ms) followed by 2) a short PRT ($\approx .78$ ms). Thus, for the lowest two elevation angles P_1, P_2 and W_1 will be available for truth for the short PRT phase coded scans. For higher elevation scans with phase coding, the estimated P_1, P_2 and W_1 would be necessary to use since long PRT truth is not available. Preliminary results indicate that use of either the truth or estimated P_1, P_2 and W_1 is unsatisfactory. Additionally, SNR will not be available as a threshold censor since leakage from the strong trip will cause weak trip power estimates to be only about 40 dB to 50 dB down from strong trip power. As mentioned above, SZ estimated moments can be censored via the variance of the velocity field. Figure 7 show the SZ recovered V_2 of Fig. 5 censored with an estimate (over 5×5 pixel grid) of velocity variance. Comparison of Fig. 7 to the truth in Fig. 5 shows that the censoring works quite well. More testing is needed.

3. SZ(8/64) and Clutter Filtering

Typically ground clutter power is removed via the use of IIR (infinite impulse response) filters which effectively remove the power around zero velocity but which also impart a phase delay which is non-linear.

This phase delay will degrade the performance of the SZ algorithm causing unacceptable biases in the $\hat{V}_2$. To show this, a 3/4 notch is applied to the spectrum of the modulation code. The resulting spectrum is IFFT'ed, recohered and magnitude of the spectrum of the resulting time series is calculated. This same process is again carried out except the original modulation code time series is first passed through an IIR clutter filter. The resulting spectra are shown in Fig. 8. The solid lines are without clutter filtering and the dashed lines are with clutter filtering. As shown by SZ99, the spectrum of the recovered weaker trip has a primary spectrum replica with 3 accompanying replicas on each side. These correspond to the 7 solid line spikes in Fig. 8. Since the 6 side replicas are symmetric about the primary replica, $\hat{V}_2$ is unbiased. The spectrum of the clutter filtered version of the modulation code does not possess such symmetry and therefore $\hat{V}_2$ will be biased. Simulation studies also show this. Thus, IIR clutter filtering and SZ phase coding are incompatible. Therefore, to effectively remove ground clutter and not adversely affect SZ recovered moments, FIR (finite impulse response) or spectral filters should be used. Currently we are investigating adaptive spectral clutter filters.

Acknowledgment This research was supported by the ROC (Radar Operations Center) of Norman OK.

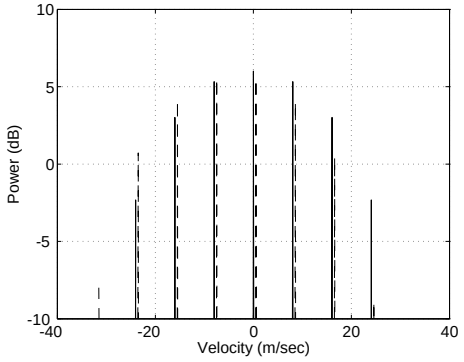

Figure 8: *Spectrum of the modulation code after 3/4 notch filter and recohering. Solid lines are without clutter filtering the dash lines are with clutter filtering.*

References

Sachidananda, M. and D.S. Zrnić, 1999: Systematic Phase Codes for Resolving Range overlaid Signals in a Doppler Weather Radar *JTECH*, **16**, 1351-1363.

Frush, C., R.J. Doviak, M. Sachidananda and D.S. Zrnić, 2002: Application of the SZ Phase Code to Mitigate Range-Velocity Ambiguities in Weather Radars, *JTECH*, **19**, 413-430.

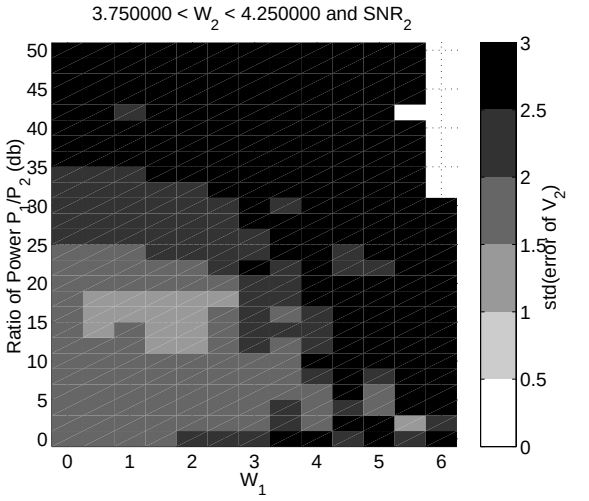

Figure 1: *The standard deviation of the errors of the recovered weak trip velocity ($\hat{V}_2$)as a function of the power ratio P_1/P_2 and the width of the stronger trip*

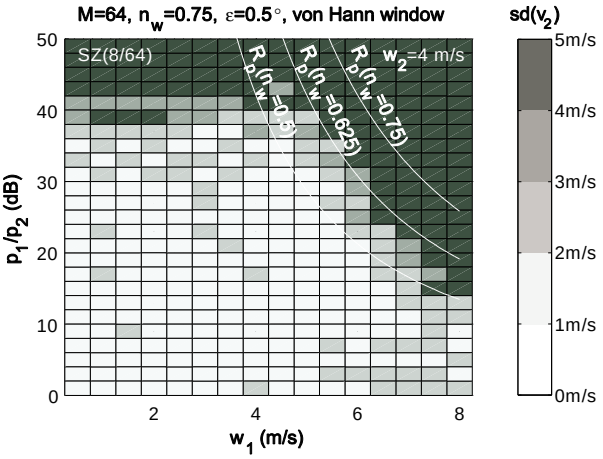

Figure 2: The standard deviation of the recovered velocity $\hat{V}_2$ as a function of the power ratio P_1/P_2 and the width of the stronger trip signal, W_1. Reproduced from Sachidananda and Zrnić (1999).

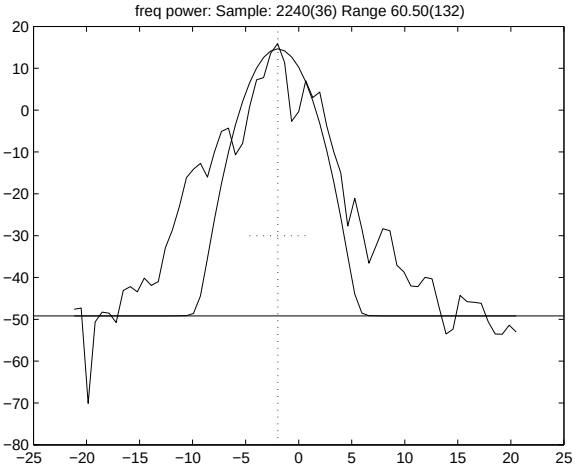

Figure 3: Experimental weather spectrum with estimated Gaussian curve overlaid.

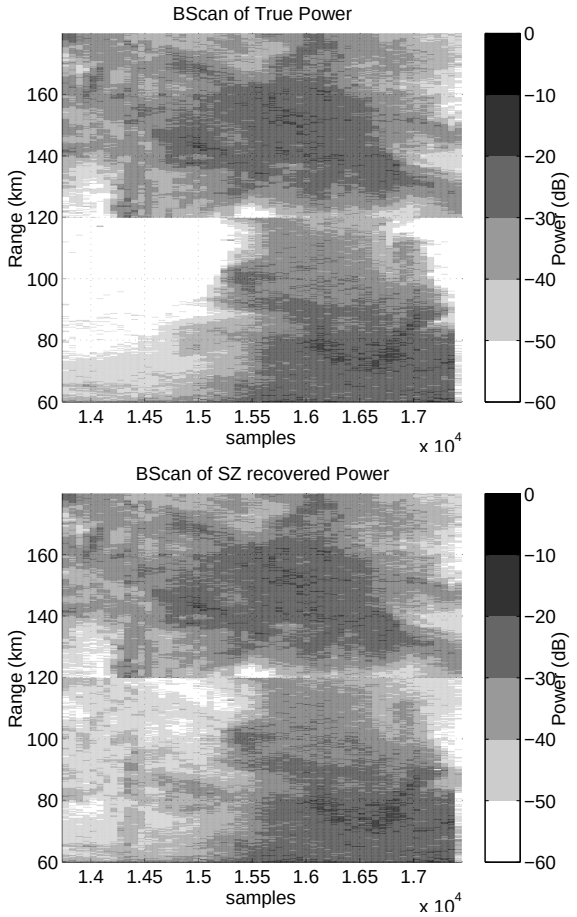

Figure 4: *Concatenated B-scans of power. The seam between the 2 separate scans can be seen at the 120 km range gate. Top Panel: Truth raw $I^2 + Q^2$ power. Bottom Panel: SZ(8/64) recovered power.*

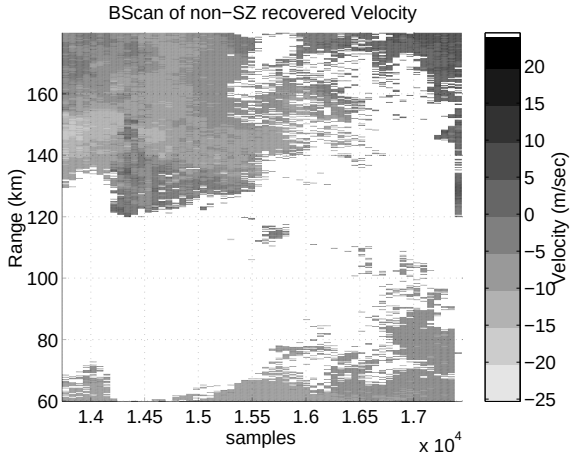

Figure 6: *Concatenated B-scans of velocity as would be measured by the current WSR-88D scanning parameters. The velocity is calculated from the truth fields of Figs. 3 and 4 (top panels) and can be compared to the SZ(8/64) recovered velocity of Fig. 4, bottom panel. The large white area is censored data.*

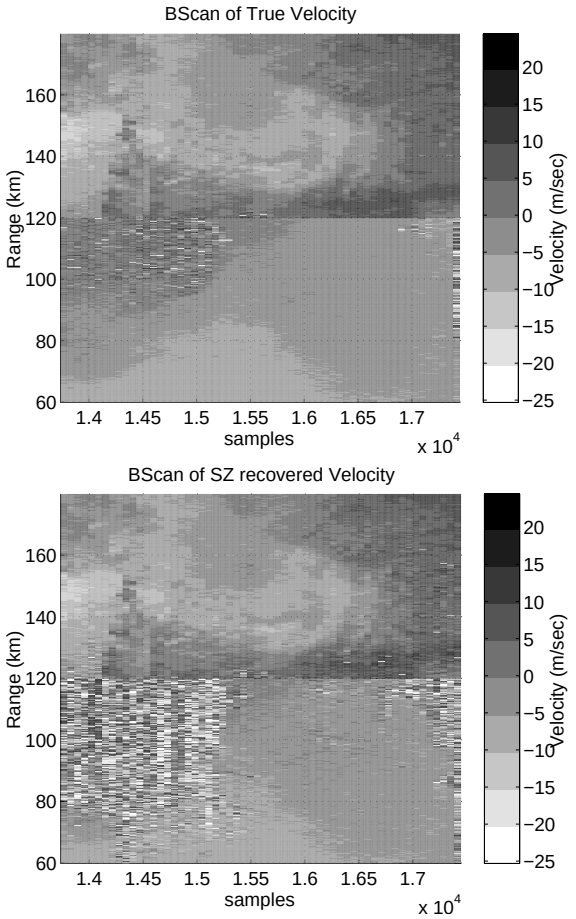

Figure 5: *Concatenated B-scans of the radial velocity. The seam between the 2 separate scans can be seen at the 120 km range gate. Top Panel: Truth velocity; Bottom Panel: SZ(8/64) recovered velocity.*

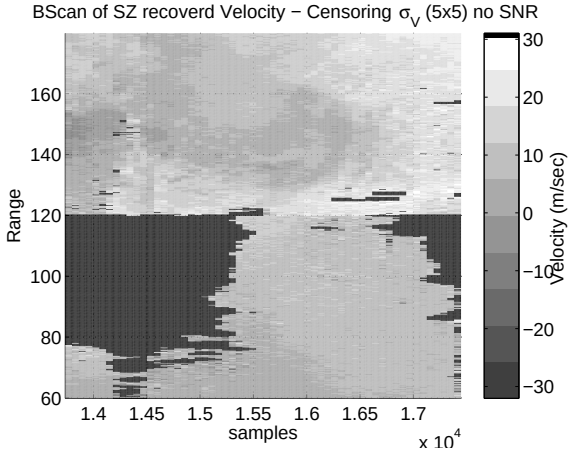

Figure 7: *Same as Fig. 4 (bottom panel) but thresholding by an areal (5×5 pixels) velocity variance estimate has been applied.*